CHEMPHYSCHEM

DOI: 10.1002/cphc.200700127

Determination of the Geometry Change of the Phenol Dimer upon Electronic Excitation

Robert Brause, Monika Santa, Michael Schmitt,* and Karl Kleinermanns*[a]

The change of the phenol dimer (PH2) structure upon electronic excitation is determined by a Franck–Condon analysis of the intensities in the fluorescence emission spectra obtained via excitation of seven different vibronic bands. A total of 547 emission band intensities are fitted, together with the changes of rotational constants upon electronic excitation of five isotopomers. These rotational constants are taken from previously published [Schmitt et al. ChemPhysChem ***2006****, 7, 1241–1249] high-resolution LIF measurements. The geometry change upon electronic excitation of the $\pi\pi^*$ state of the donor moiety can be described by a strong shortening of the hydrogen bond, a shortening of the CO bond in the donor moiety, an overall symmetric expansion of the donor phenol ring, and a nearly unchanged acceptor moiety. The resulting geometry changes are interpreted on the basis of ab initio calculations.*

1. Introduction

In a recent publication the intermolecular structure of the phenol dimer in the ground and the lowest electronically excited state was elucidated using the rotational constants obtained via rotationally resolved laser-induced fluorescence spectroscopy of five different isotopomers.[1] While in principle the determination of molecular structures in different electronic states from inertial parameters is a straightforward procedure, one has to pay considerable attention to possible model errors, when the number of geometry parameters exceeds the number of rotational constants. For a complete fit of the phenol dimer geometry in internal coordinates 72 parameters (25 distances, 24 angles and 23 dihedral angles) have to be determined, while only 15 rotational constants (from five isotopomers) are known. Under the assumption of planar monomer moieties in the cluster, 18 of the 23 dihedral angles can be fixed. More restrictions on the geometries of the monomer moieties in both electronic states [both phenol geometries are completely unaltered upon cluster formation in the ground state, or geometry change upon excitation occurs only on the (locally) excited moiety, etc.] greatly enhance the risk of being trapped in a local minimum when fitting the cluster structure. More (independent) data are urgently needed for a reliable determination of the dimer structure.

An alternative approach to excited state structures is facilitated by the Franck–Condon (FC) principle. According to the FC principle the probability of a vibronic transition and thus the relative intensity of a vibronic band depends on the overlap integral of the vibrational wavefunctions of both electronic states. This overlap integral is determined by the relative shift of the two potential energy curves connected by the vibronic transition along the normal coordinates Q of both states. Thus, via the calculated FC factors, the structural change upon electronic excitation can be deduced from the experimentally determined intensity pattern.[2–5] Even though the FC principle does not allow for an independent determination of the structure in each of the states, it allows to enumerate geometry changes upon electronic excitation.

In the phenol dimer, dispersive interactions between the aromatic rings play an important structural role, while for most hydrogen-bonded phenol–X clusters (X = H_2O,[6–20] CH_3OH,[21–23] N_2,[24–29] NH_3,[30–39] CO[24,40]) the hydrogen bond is by far the most important structure determining parameter.

Extensive experimental work on the phenol dimer has been performed using resonant multi-photon ionisation in the region of the donor and the acceptor origin,[41,42] zero-kinetic electron (ZEKE) spectroscopy,[43] as well as hole burning spectroscopy.[44] Ohashi et al. showed via photodissociation spectroscopy, that the cluster ion is comprised of a cationic and a neutral moiety with little resonance interaction between both.[45] Ionisation-loss stimulated Raman spectroscopy was used by Hartland et al. to compare vibrational frequency shifts for both donor and acceptor phenol with the hydrogen bond strength.[46] IRUV double-resonance spectroscopy and stimulated Raman–UV double-resonance spectra of the phenol dimer were published by Ebata et al.[47] For the dimer, they found that the IR intensity of the OH-stretching vibration of the donor moiety is four times larger than that of the acceptor moiety. Ebata et al. investigated IVR from OH stretching vibrations of the phenol dimer using picosecond IR–UV pump-probe spectroscopy.[48] They found a strong site-dependence of the IVR rate. IVR of the donor site was found to occur much

[a] *Dr. R. Brause, M. Santa, Priv.-Doz. Dr. M. Schmitt, Prof. Dr. K. Kleinermanns*
Heinrich-Heine-Universität
Institut für Physikalische Chemie I
40225 Düsseldorf (Germany)
Fax: (+49) 211-81-15195
E-mail: mschmitt@uni-duesseldorf.de
kleinermanns@uni-duesseldorf.de

Supporting information for this article is available on the WWW under http://www.chemphyschem.org or from the author.

faster (5 ps) than of the acceptor site (14 ps). Felker[49] and Connell et al.[50] determined mean rotational constants of ground and excited state using rotational coherence spectroscopy (RCS). Later Weichert et al.[51] performed an RCS experiment on the dimer with higher temporal resolution and were able to extract the rotational constants of ground and excited states separately. Nakagawa et al. investigated the *m*-chlorophenol dimer using R2PI spectroscopy. In sharp contrast to all findings for the phenol dimer they postulate a stacked structure for the *m*-chlorophenol dimer.[52]

The ground state and the cationic state of PH2 was fully optimised by Ghosh and Miyoshi at Hartree–Fock level of theory.[53] Hobza et al.[54] performed ab initio calculations on the RIMP2/TZVPP level of theory and found good agreement with the experimental inertial parameters from ref. [51].

Experimental and Computational Methods

Experiment

The experimental setup for the dispersed fluorescence (DF) spectroscopy is described in detail in refs. [44,55]. In brief, phenol was evaporated at 390 K and co-expanded through a pulsed nozzle with a 500 μm orifice (General Valve) into the vacuum chamber using helium as carrier gas. The output of a Nd:YAG (Spectra Physics, Quanta Ray Indi) pumped dye laser (Lambda-Physik, FL3002) was frequency doubled and crossed perpendicularly with the molecular beam. The fluorescence light was collected perpendicularly to laser and molecular beams and was imaged on the entrance slit of a 1 m monochromator (Jobin Yvon, 2400 grooves/mm blazed at 400 nm for first order). The dispersed fluorescence was recorded by an intensified CCD camera (Flamestar II, LaVision). This allows to image simultaneously a DF spectrum of about 600 cm^{-1}. Accordingly, the relative intensities in our DF spectra do not vary with laser power. Only the intensity of the excited band is perturbed by scattered light. Thus, we normalise relative intensities with respect to the strongest band in the spectrum other than the resonance fluorescence band. The intensity uncertainty of the whole detection system was checked by shifting a particular fluorescence line over the CCD chip by changing the grating position. The observed intensity error was 10% at maximum.

Ab initio Calculations

Ab initio calculations at the Møller-Plesset second order perturbation (MP2) level of theory within the resolution-of-the-identity (RI) approximation have been carried out using the TURBOMOLE program package (Version 5.8).[56–61] Ahlrich's valence triple ζ basis sets were used for the RIMP2 (TZVPPP) calculations.[58,62] MP2 calculations were also performed with the GAUSSIAN03 program suite.[63] Dunning's correlation consistent valence triple ζ basis set with polarisation functions (cc-pVTZ)[64] as well as Pople's triple ζ basis set with polarisation functions [6-311G(d,p)][65] were applied. With both basis sets the geometry was optimised but with the Pople basis set we included additionally a counterpoise correction to account for the basis set superposition error.

Second-order approximate coupled cluster (CC2) calculations within the resolution-of-the-identity (RI) approximation were accomplished with the TURBOMOLE program package (Version 5.8)[59–61,66–69] for the ground as well as for the first excited state. As appropriate basis set Ahlrich's valence triple ζ with one set of polarisation functions per atom was used (TZVP).[58,62] In order to ensure that the optimised structure is a real minimum we calculated numerically the second derivatives. We obtained no imaginary frequencies for all normal modes. Thus, the optimised structures are minima structures. All calculations were performed on a Sun Opteron Cluster.

Franck–Condon Fit of the Structural Change

The change of a molecular geometry upon electronic excitation can be determined from the intensities of absorption or emission bands using the FC principle. According to the FC principle the relative intensity of a vibronic band depends on the overlap integral of the vibrational wavefunctions of both electronic states. The fit has been performed using the program FCFIT, which has been developed in our group and described previously.[2]

2. Results

Ab initio Calculations

The ground state structure of PH2 was optimised at the MP2/cc-pVTZ, MP2/6-311G(d,p) level (optimisation performed, using BSSE corrected gradients with the counterpoise (cp) method of Boys and Bernardi[70]), RIMP2/TZVPPP, and RICC2/TZVP levels of theory. The S_1 state geometry was optimised at the RICC2/TZVP level of theory. For both ground and excited state, the harmonic vibrational frequencies were calculated, using analytical or numerical second derivatives of the potential energy. The resulting geometry parameters are presented in Table 1. The atomic numbering in Table 1 refers to Figure 1.

MP2, RIMP2, and RICC2 calculations are capable of describing the structure which is affected by dispersive interactions. Hence, the rotational constants of these calculations deviate at most 8% from the experimental results. With the counterpoise correction one can even improve these results to deviations of the rotational constants below 2%, cf. Table 1.

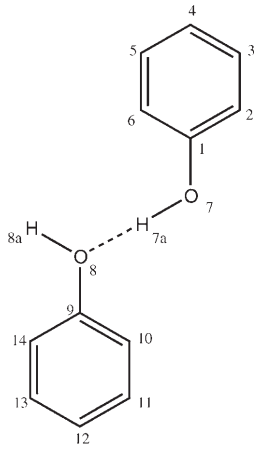

Figure 1. Atomic numbering of the phenol dimer. Both monomer moieties of the dimer are drawn planar for reason of clarity. This does not bear any relation to the true structure.

Since ground and excited state geometry and the respective Hessian must be calculated at the same level of approximation, we used the coupled cluster method because CASSCF(S_0/S_1) fails to describe accurately the geometry in both states.

The binding energies of the phenol dimer in the ground and excited state have been calculated at the RICC2/TZVP level of theory including the zero-point energies to be 32.3 kJ mol^{-1} and 38.8 kJ mol^{-1}, respectively. Table 2 presents the vibrational frequencies of the 6 intermolecular normal modes of PH2 cal-

Table 1. S_0 state geometry parameters of the phenol dimer, calculated at the MP2/cc-pVTZ, MP2/6-311G(d,p) counterpoise-corrected, RIMP2/TZVPPP, RICC2/TZVP level of theory, and from a structural fit to the ground state rotational constants of 5 isotopomers published in ref. [1]. In parentheses: relative deviations from the experimental values in %. The atomic numbering refers to Figure 1. All bond lengths are given in Å. Angles *a* and dihedral *d* are given in degrees.

S_0	MP2 cc-pVTZ	MP2(cp-corr.) 6-311G(d,p)	RIMP2 TZVPPP	RICC2 TZVP	Exp.[1]
A″[MHz]	1534(8.3)	1392(1.8)	1519(7.2)	1497(5.6)	1416.99
B″[MHz]	308(1.8)	312(0.5)	311(0.8)	314(0.2)	313.51
C″[MHz]	290(0.7)	282(2.1)	292(1.4)	293(1.7)	288.11
ΔI [uÅ^2]	−230(7.2)	−195(9.1)	−224(4.4)	−226(5.3)	−214.54
Donor					
C1–C2	1.396	1.402	1.393	1.399	1.391
C2–C3	1.391	1.396	1.389	1.392	1.394
C3–C4	1.394	1.400	1.392	1.397	1.395
C4–C5	1.392	1.398	1.390	1.394	1.395
C5–C6	1.394	1.399	1.392	1.396	1.399
C6–C1	1.398	1.403	1.395	1.400	1.392
ϕ ring	1.394	1.400	1.392	1.396	1.394
C1–O7	1.361	1.362	1.359	1.368	1.374
O7–H7a	0.971	0.967	0.969	0.976	0.957
Acceptor					
C9–C10	1.392	1.399	1.390	1.394	1.392
C10–C11	1.391	1.396	1.389	1.394	1.399
C11–C12	1.394	1.400	1.392	1.396	1.395
C12–C13	1.392	1.397	1.390	1.394	1.395
C13–C14	1.393	1.399	1.391	1.396	1.394
C14–C9	1.391	1.398	1.389	1.392	1.391
ϕ ring	1.392	1.398	1.390	1.394	1.394
C9–O8	1.381	1.377	1.378	1.389	1.374
O8–H8a	0.964	0.962	0.961	0.968	0.957
Inter					
H7a–O8	1.881	1.995	1.877	1.863	2.369
a(**O7–H7a–O8**)	167.6	171.1	167.8	168.6	150.5
a(**C9–O8–H7a**)	114.1	122.7	115.3	114.0	139.8
d(**O8–H7a–O7–C1**)	84.0	113.5	82.0	86.2	9.4
d(**C9–O8–H7a–O7**)	6.6	−60.0	5.3	−0.2	62.8
d(**C10–C9–O8–H7a**)	−34.7	18.4	−33.2	−34.6	−2.0

culated at the MP2/cc-pVTZ, MP2(cp-corrected)/6-311G(d,p), RIMP2/TZVPPP, and RICC2/TZVP level of theory.

The respective intermolecular vibrations (and the intramolecular ones as well) should be inspected as animated graphs with a viewer like Molden or Molekel.[71,72] The Gaussian.log and TURBOMOLE.molf files, which contain the normal mode analyses can be downloaded from our homepage.[73] The quoted calculated frequencies are unscaled and compared to the experimental frequencies in Table 2.

Table 2. Calculated harmonic ground and excited state vibrational frequencies of the six intermolecular normal-modes of PH2 at different levels of theory. All frequencies are given in cm^{-1}.

	S_0					S_1	
Assignment	RIMP2 TZVPPP	MP2 cc-pVTZ	MP2(cp-corr.) 6-311G(d,p)	RICC2 TZVP	Exp.[44]	RICC2 TZVP	Exp.[44]
ν_1	23	11	9	24	9	23	7
ν_2	24	23	13	28	18	31	12
ν_3	44	37	21	41	34	40	15
ν_4	73	74	59	78	44	81	23
ν_5	78	78	64	82	50	89	30
$\nu_1(\sigma)$	127	127	106	130	110	138	119

In Figure 2 the frontier orbitals of PH2 calculated at the RICC2 level are depicted. The molecular orbitals have large

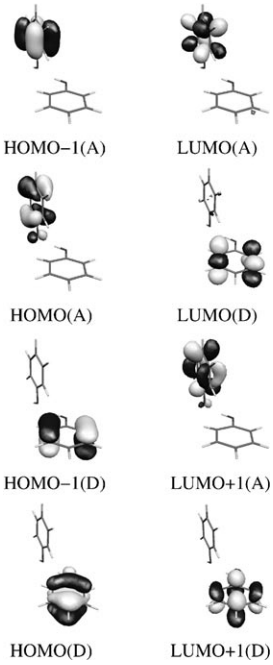

Figure 2. Frontier orbitals of the phenol dimer calculated with the RICC2/TZVP level of theory.

coefficients either at the donor or at the acceptor moiety. The excitations to the first and the second excited singlet state are localised to nearly pure donor or acceptor type (weights ~85 %), cf. Table 3. Thus, we exclude significant charge-transfer character in the lowest singlet excitations within the Franck–Condon region.

Experimental Results

Figure 3 shows the fluorescence excitation spectrum in the donor origin region of PH2. The peaks labelled with an asterisk in Figure 3 were excited to obtain the DF spectra that are shown in Figures 4 and 5. The assignment of these absorption bands to specific vibrational modes in the excited state was made on the basis of the propensity rule from the intensities in the emission spectra and are given in the inset of Figure 3 and in Table 4. The assignment will be explained below, togeth-

Table 3. Weights of the frontier orbitals, depicted in Figure 2, for the excitations to the first and second excited singlet state of the phenol dimer.

S_1	
HOMO(D)→LUMO(D)	68%
HOMO−1(D)→LUMO+1(D)	17%
HOMO(D)→LUMO(A)	9%
S_2	
HOMO(A)→LUMO(A)	59%
HOMO−1(A)→LUMO+1(A)	25%
HOMO(A)→LUMO(D)	5%

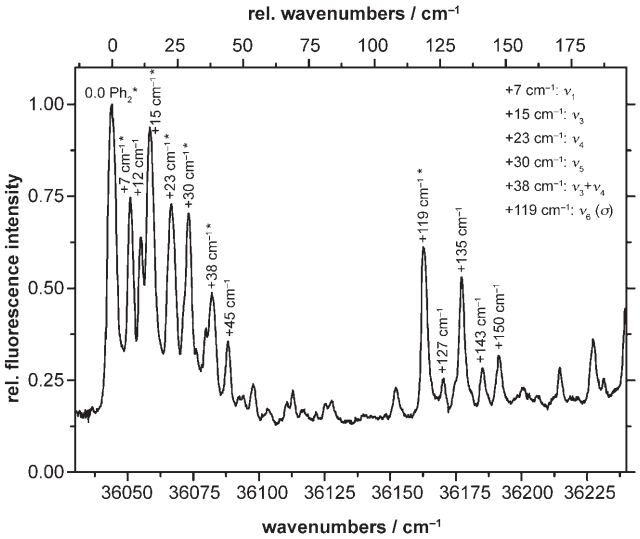

Figure 3. LIF spectrum of the phenol dimer in the region of the donor origin. The peaks labelled with an asterisk were pumped to obtain the respective dispersed fluorescence spectra, cf. Figures 4 and 5.

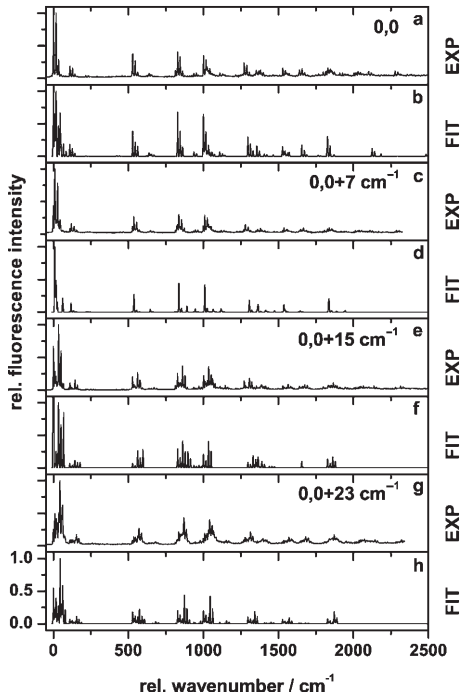

Figure 4. Comparison of experimental and simulated fluorescence emission spectra of the phenol dimer pumped via 0,0, 0,0+7 cm^{-1}, 0,0+15 cm^{-1}, and 0,0+23 cm^{-1}. The respective upper traces show the experimental DF spectra and the lower spectra are the fit results. The simulated intensities are convoluted with a Gauss profile with a band width at half intensity of 5 cm^{-1} and plotted by using experimental wavenumbers to facilitate the comparison of the intensities.

Table 4. Intensities of emission bands, relative to the most intense band of the respective spectrum (not including the resonance fluorescence band) after excitation of different S_1 vibrations. The transition marked with an asterisk is the strongest transition in the respective emission spectrum and is utilised to identify the S_1 mode used for excitation.

S_1 Transition	0,0	0,0+7	0,0+15	0,0+23	0,0+30	0,0+38	0,0+119
ν_1	0.0752	1.0000*	0.2886	0.4918	0.1540	0.0614	0.0000
ν_2	1.0000	0.1948	0.2099	0.4187	0.6263	0.3168	0.1910
ν_3	0.2857	0.0000	1.0000*	0.4861	0.4712	0.3883	0.0684
ν_4	0.0427	0.2184	0.0000	1.0000*	0.0000	0.2776	0.0000
ν_5	0.0585	0.0000	0.0000	0.0000	1.0000*	0.0000	0.0166
$\nu_3+\nu_4$	0.0000	0.0000	0.0000	0.0000	0.0000	1.0000*	0.0000
σ	0.1835	0.0824	0.1104	0.0873	0.0505	0.0679	1.0000*

er with a discussion of the respective ground state vibrations.

The first trace of Figure 4 shows the fluorescence emission spectrum, obtained via excitation of the vibrationless origin 0,0. The assignments given are based on the ab initio calculations described earlier in this Section. The calculated frequencies for the ground state intermolecular vibrations that were used for the assignment are summarised in Table 2.

The strongest band in the emission spectrum after excitation at 0,0+7 cm^{-1} (trace c of Figure 4) is found at 9 cm^{-1} and can be assigned on the basis MP2/cc-pVTZ calculations to the intermolecular ν_1 vibration. The corresponding computed frequency value from the MP2 calculation is quite close (11 cm^{-1}) (see Table 2). Combination bands with the vibrations ν_2, σ, 6a-(a,d)[1], 1(d), 12(a), and 13(d) can be identified. The assignment of the 7 cm^{-1} band in the absorption spectrum to ν_1 in the S_1 state therefore appears reasonable.

Excitation at 15 cm^{-1} (trace e of Figure 4) results in a long progression up to the third overtone of a band at 34 cm^{-1} and combination bands with the modes σ, 15(d), 6a(a,d), 1(d), 12(a), and 13(d). The MP2 calculations allow a straightforward assignment of the S_1 vibration at 15 $cm^{-1}$to mode ν_3. Trace g of Figure 4 represents the fluorescence emission spectrum originating from the UV-absorption band at 0,0+23 cm^{-1}. The strongest band in this spectrum is located at 44 cm^{-1} and is assigned to the fundamental of vibration ν_4. This assignment is again obtained by the propensity rule showing high intensities

[1] *The declaration (a), (d), or (a,d) indicates the localisation of the corresponding vibration: acceptor, donor, or non-local.*

in the fundamental mode as well as in the combination bands of the ν_4 with several intermolecular and intramolecular vibrations.

The experimental spectrum of the band located at 0,0 + 30 cm^{-1} is shown in Figure 5, trace a. The most prominent band in this spectrum arises at 50 cm^{-1} and consecutively shows high Franck–Condon factors in combination bands with almost all fundamentals observed in the spectrum. The band is assigned to the fundamental of the normal mode ν_5.

The most intense peak in the DF spectrum at 0,0 + 38 cm^{-1} is located at 76 cm^{-1} and is attributed to the combination band of the intermolecular vibrations ν_3 and ν_4, cf. trace c of Figure 5. This assignment is proven by the fact that the combination bands with intramolecular modes like 6a(a,d) and 1(d) are the most intense ones compared to the other combination bands like eg. $\nu_2\nu_4$6a(a,d).

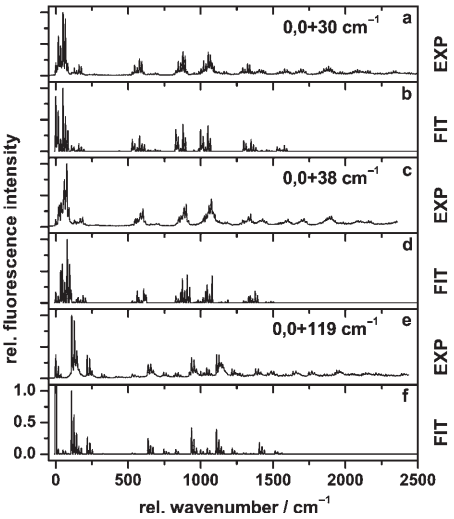

Figure 5. Comparison of experimental and simulated fluorescence emission spectra of the phenol dimer pumped via 0,0 + 30 cm^{-1}, 0,0 + 38 cm^{-1}, and 0,0 + 119 cm^{-1}.

Excitation at 119 cm^{-1} (trace e of Figure 5) results in a long progression up to the third overtone of a band at 109 cm^{-1} and combination bands with the modes ν_2, ν_3, ν_5, 6a(a,d), 1(d), 12(d), and 13(d). This vibration can be unambiguously identified as the intermolecular stretch mode σ, cf. Table 2.

The assignments for the intermolecular modes in the ground as well as the excited state are in best agreement with the assignment in ref. [44].

Geometry Fit Results

The geometry changes of PH2 are fitted, using the program FCFIT, so that the line intensities in the emission spectra are well described. 547 line intensities from three fluorescence emission spectra and the rotational constant changes of five different isotopomers were used for the fit. Emission spectra have been obtained from excitation of the vibrationless 0,0, ν_1, ν_3, ν_4, ν_5, $\nu_3 + \nu_4$, and σ. All intermolecular normal modes were taken as displacement vectors for the fit. Additionally, the ring modes 6a(a,d), 1(d), 12(d) and the 13(d) vibration were included in the fit, because all modes show up in the DF spectra as fundamentals as well as combination bands with the respective prominent intermolecular vibrations. Thus, the ten motions which form the basis for the displacements upon electronic excitation are ν_1, ν_2, ν_3, ν_4, ν_5, σ, 6a(a,d), 1(d), 12(d) and 13(d). They can be viewed as animated graphs with a viewer like Molden or Molekel,[71,72] after download of the Gaussian.log and TURBOMOLE.molf files from our homepage[73] or from the Supporting Information. The use of a selected sub-ensemble of normal modes as basis for the displacements is forced by the difficulty to assign a sufficient number of vibrations in the electronically excited state. This selection has to be performed carefully, in order to avoid artificial displacement effects by consideration of similar modes. First of all, a simulation of the intensities of the emission bands was performed, using the geometries and the Hessian matrices from the RICC2/TZVP calculations. The simulations from the RICC2 calculations are given in the Supporting Information, or alternatively can be downloaded from our homepage.[73] Although the overall performance of these simulations seem not to be too bad, there are severe deviations between the experimental and simulated intensities.

After the simulations with the unchanged ab initio geometries for each electronic state, we performed combined fits of the intensities (547 data-points) of the vibrations, overtones and combination bands in the spectra of Figures 4 and 5 and the changes of the rotational constants of five isotopomers by displacing the S_1-state geometry along the ten normal modes described above. The results are shown in the traces below the respective experimental spectra in Figures 4 and 5. Close inspection of all emission spectra shows that the intensity pattern is well reproduced upon displacement of the S_1 geometry.

Table 5 summarises the results for the S_1 displacements obtained from the Franck–Condon fit described above. The first column presents the results for the geometry changes upon electronic excitation as obtained from the RICC2 calculations. The second column shows the results for the geometry changes from the Franck–Condon fit to 547 fluorescence emission bands and to the changes of the rotational constants of five isotopomers. The third column gives the experimentally determined rotational constant changes and the results for the geometry changes from the fit to the rotational constants of five isotopomers of PH2 using *pKrFit* by Schmitt et al.[1]

Both phenol rings remain planar upon electronic excitation. The donor ring expands nearly symmetrically whereas the acceptor ring changes are almost zero indicating a local excitation in the donor moiety. The C–O bond length in the donor ring (**C1**–**O7**) decreases while the respective bond in the acceptor moiety (**C9**–**O8**) increases, but to a smaller extent. The hydrogen bond **O8**–**H7a** is shortened considerably. The other intermolecular parameters (angles and dihedrals) change only slightly.

In Table 6 the center of mass (COM) distances of the monomer moieties are displayed for the ground and excited state of the five used isotopomers and compared to the experimentally

Table 5. Comparison of the geometry changes of the phenol dimer upon electronic excitation from a RICC2/TZVP study, from the Franck–Condon fit, and from a structural fit (model 1) to the rotational constants of 5 isotopomers published in ref. [1]. The atomic numbering refers to Figure 1. All bond length changes are given in pm. Changes of the angles *a* and dihedrals *d* are given in degrees.

S_1–S_0	RICC2	FCfit	Exp.[1]
ΔA [MHz]	10.4	10.8	10.71
ΔB [MHz]	−1.4	−6.0	−5.31
ΔC [MHz]	−0.7	−4.5	−5.82
Donor			
ΔC1–C2	2.3	2.9	2.2
ΔC2–C3	4.0	4.5	1.2
ΔC3–C4	2.4	2.9	1.3
ΔC4–C5	3.2	3.6	1.4
ΔC5–C6	3.3	3.9	1.9
ΔC6–C1	3.7	5.1	1.3
$\Delta\phi$ ring	3.2	3.8	1.6
ΔC1–O7	−1.7	−2.0	−5.7
ΔO7–H7a	1.1	1.2	0.3
Acceptor			
ΔC9–C10	−0.1	0.2	−2.9
ΔC10–C11	0.0	0.3	−2.5
ΔC11–C12	0.0	0.7	−1.1
ΔC12–C13	0.0	0.3	−1.5
ΔC13–C14	0.0	0.1	−1.0
ΔC14–C9	−0.1	0.5	−1.2
$\Delta\phi$ ring	0.0	0.4	−1.7
ΔC9–O8	0.4	0.6	0.8
ΔO8–H8a	0.0	0.0	0.0
Inter			
ΔH7a–O8	−8.9	−7.7	−7.9
ΔC10–H···donor ring[a]	1.7	9.6	38.8
Δ*a*(O7–H7a–O8)	−0.5	1.8	29.5
Δ*a*(C9–O8–H7a)	−1.0	1.1	−35.7
Δ*d*(O8–H7a–O7–C1)	20.4	9.8	37.5
Δ*d*(C9–O8–H7a–O7)	−20.0	−7.7	165.9
Δ*d*(C10–C9–O8–H7a)	−4.8	−10.1	73.0

[a] Distance to the geometric center of the donor moiety.

Table 6. COM distances [pm] of the five observed isotopomers of PH2 in the ground and electronic excited states obtained by the Franck–Condon fit. In parentheses the deviations of the experimental values obtained by Schmitt et al.[1] are given in %.

	S_0	S_1
h6–h6[a]	519.605(1.1)	523.695(1.2)
d1–d1[a]	520.657(0.2)	524.635(0.2)
d1–h6[b]	521.606(0.4)	525.716(0.6)
d6–d6	522.526(0.9)	526.723(0.9)
13c–13c[c]	518.231(1.1)	522.209(1.3)

[a] Hydroxy hydrogens substituted. [b] Donor moiety at the hydroxy group deuterated. [c] **C1** and **C9** according to Figure 1 substituted.

obtained ones from ref. [1]. The COM distances for all isotopomers in both states are very well described by the structures obtained by the Franck–Condon fit, cf. Table 6. The deviations are all about 1%.

3. Conclusions

The intermolecular structure of the phenol dimer in the electronic ground state can be described as hydrogen bonded, with one phenol moiety acting as proton donor and the other as proton acceptor. The orientation of the two monomer moieties differs, from what can be expected from a pure translinear arrangement as found for example, for the phenol-water cluster. This deviation is a consequence of the additional dispersive interactions between the two aromatic rings, as has already been pointed out by Hobza et al.[54] Although, we used the same method (RIMP2) with the same basis set (TZVPP) as well as a smaller (TZVP) and a bigger one (TZVPPP), we could not reproduce the minimum structure described in ref. [54]. The rotational constant A is always found to be above 1500 MHz according to our calculations (cf. Table 1), whereas Hobza et al. reported an A constant of 1453 MHz. We tried different starting geometries for the optimisation, but all ended up in the same minimum structure. Thus, we believe that the structure of the ground state which is reported herein is the true global minimum. All ab initio calculations taking dispersive interactions properly into account (MP2, RIMP2, and RICC2) describe, quantitatively well, the ground-state structure. As a measure for the quality of the theoretical results we take the deviations from the experimentally determined rotational constants and inertial defect, cf. for Table 1. The best result is obtained by the MP2 method using the counterpoise correction in the gradient-step. Unfortunately, counterpoise-corrected gradients are currently only available through the Gaussian03 package. Implementation of BSSE-corrected gradients in the TURBOMOLE program package would improve the results for the excited state optimisations using the coupled-cluster module considerably, cf. the improvement for the MP2 method.

The structure of PH2 has been calculated by the RICC2 method for the ground state as well as for the excited state. It is the first time to our knowledge that an optimised excited state structure for PH2 is published which is based on a method that holds for dispersive interactions. As can be seen from Table 5 the changes of the geometry upon electronic excitation occur only in the intramolecular bonding motif of the donor moiety and the intermolecular coordinates. This finding can be traced back to the local excitation of PH2, cf. Table 3. In ref. [1] this assumption was made as basis for "model 2". In Table 5 the experimental values, using "model 1" from ref. [1] [donor and acceptor geometries kept fixed at the CIS/6-311G-(d,p) optimised structure] are compared to the results of the Franck–Condon fit and the RICC2 calculations. Table 5 clearly shows that the geometry changes of the donor and acceptor moiety are about the same size in opposite directions. This is due to the model limitations which have been stated in ref. [1]: "The results for the excited-state structure depend strongly on the chosen model, and need further refinement using information from isotopomers other than the ones used in this study, to estimate the changes in the monomer moieties upon electronic excitation". In a case like this, with an insufficient number of different isotopomers for a full structure fit, the ad-

ditional consideration of FC activity helps to remove possible ambiguities. Since the Franck–Condon fits presented here use the full information from the rotational constants, in combination with the intensities of a large number of vibronic transitions, this fit yields more reliable structures, than a fit to the rotational constants alone.

Based on our Franck–Condon fit the intermolecular binding motif changes upon electronic excitation to a smaller extent than predicted by Schmitt et al. The decrease of the intermolecular bond length **H7a**–**O8** is of the same magnitude. However, the intermolecular angles and dihedrals change much less upon electronic excitation in the framework of the Franck–Condon model used here. The next difference is found for the structural changes of the acceptor moiety. We find an almost unaltered acceptor ring in contrast to an overall contraction of the acceptor ring in the model of Schmitt et al. The **C9**–**O8** bond length increase has about the same magnitude (0.6, 0.8 pm) in both models. This result can be understood by looking at the intermolecular bond **H7a**–**O8**. The intermolecular bond gains more electron density from the O8 atom, thus weakening the bond **C9**–**O8**. In the donor ring both models predict an overall expansion which is two times as large in the Franck–Condon model, cf. $\Delta\phi$ ring in Table 5. The **C1**–**O7** bond length is shortened in both models. In the model of Schmitt et al. the value of the **C1**–**O7** bond length is three times larger than in the Franck–Condon fit. The **O7**–**H7a** bond length increases in both models. The decrease of the **C1**–**O7** bond length and the increase of the **O7**–**H7a** bond length can again be traced back to the shortening of the intermolecular bond **O8**–**H7a**.

Figure 6 illustrates the above described geometry changes. In the electronic ground state (red) and the excited state

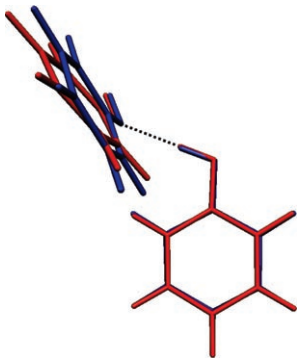

Figure 6. Superposition of the S_0 and the S_1 state structures obtained by the FC fit. The S_0 structure is drawn in red and S_1 structure in blue. The FC fit is based on the ground state geometry obtained from the RICC2/TZVP calculations.

(blue), the two rings are virtually perpendicular, thus prohibiting any considerable $\pi\cdots\pi$ interaction of the two aromatic systems. The van der Waals forces between the two phenol moieties are governed by C–H$\cdots\pi$ interactions, which decrease upon electronic excitation. This decrease can be traced back to a stronger hydrogen bond in the excited state, which shortens the O–H···O bond length. Due to an increased steric hindrance between the two rings, the acceptor moiety tilts away from the ground state orientation, thus increasing effectively the mean C–H$\cdots\pi$ distance.

One has to keep in mind, that the Franck–Condon fit uses, as basis for the displacements, normal modes which are predominantly localised in the donor moiety. The only exception is the mode 6a, which is more or less delocalised over both rings. This is due to the fact, that the acceptor modes show virtually no FC activity in the whole spectral range. Therefore, the rather small geometry changes, which are found in the acceptor moiety might also be due to this deficient displacement basis. On the other hand no severe deviations of the experimental FC factors from the calculated ones are observed, which proves that these displacements are less important displacement vectors for the geometry changes.

The above findings clearly show, that models for the monomer structures that are deduced from non-correlated ab initio structural calculations can be considerably deficient. In this case the additional information from FC fits, using the displacement vectors along normal modes of the monomer moieties in the cluster greatly improves the quality of the excited state structures.

Acknowledgements

This work has been performed in the SFB 663 (TPA2 and A4), Universität Düsseldorf and was printed upon its demand with financial support from the Deutsche Forschungsgemeinschaft. The authors like to thank the Universitätsrechenzentrum Köln for the granted computing time on the Sun Opteron cluster "clio".

Keywords: ab initio calculations · fluorescence spectroscopy · Franck–Condon analysis · hydrogen bonds · laser spectroscopy

[1] M. Schmitt, M. Böhm, C. Ratzer, D. Krügler, K. Kleinermanns, I. Kalkmann, G. Berden, W. L. Meerts, *ChemPhysChem* **2006**, *7*, 1241 – 1249.
[2] D. Spangenberg, P. Imhof, K. Kleinermanns, *Phys. Chem. Chem. Phys.* **2003**, *5*, 2505 – 2514.
[3] P. Imhof, D. Krügler, R. Brause, K. Kleinermanns, *J. Chem. Phys.* **2004**, *121*, 2598 – 2610.
[4] R. Brause, M. Schmitt, D. Krügler, K. Kleinermanns, *Mol. Phys.* **2004**, *102*, 1615 – 1623.
[5] R. Brause, D. Krügler, M. Schmitt, K. Kleinermanns, A. Nakajima, T. Miller, *J. Chem. Phys.* **2005**, *123*, 224311.
[6] H. Abe, N. Mikami, M. Ito, *J. Phys. Chem.* **1982**, *86*, 1768 – 1771.
[7] A. Sur, P. M. Johnson, *J. Chem. Phys.* **1986**, *84*, 1206 – 1209.
[8] R. J. Stanley, A. W. Castleman, Jr., *J. Chem. Phys.* **1991**, *94*, 7744 – 7756.
[9] R. J. Lipert, S. D. Colson, *J. Chem. Phys.* **1988**, *89*, 4579 – 4585.
[10] M. Schütz, T. Bürgi, S. Leutwyler, T. Fischer, *J. Chem. Phys.* **1993**, *98*, 3763 – 3776.
[11] M. Schütz, T. Bürgi, S. Leutwyler, *J. Mol. Struct. Theochem* **1992**, *95*, 117 – 132.
[12] G. Berden, W. L. Meerts, M. Schmitt, K. Kleinermanns, *J. Chem. Phys.* **1996**, *104*, 972 – 982.
[13] M. Gerhards, M. Schmitt, K. Kleinermanns, W. Stahl, *J. Chem. Phys.* **1996**, *104*, 967 – 971.
[14] M. Schmitt, C. Jacoby, K. Kleinermanns, *J. Chem. Phys.* **1998**, *108*, 4486 – 4495.
[15] R. M. Helm, H. P. Vogel, H. J. Neusser, *J. Chem. Phys.* **1998**, *108*, 4496 – 4504.

[16] T. Ebata, M. Furukawa, T. Suzuki, M. Ito, *J. Opt. Soc. Am. B* **1990**, *7*, 1890 – 1897.
[17] O. Dopfer, G. Reiser, K. Müller-Dethlefs, E. W. Schlag, S. D. Colson, *J. Chem. Phys.* **1994**, *101*, 974 – 989.
[18] T. Watanabe, T. Ebata, S. Tanabe, N. Mikami, *J. Chem. Phys.* **1996**, *105*, 408 – 419.
[19] S. Tanabe, T. Ebata, M. Fujii, N. Mikami, *Chem. Phys. Lett.* **1993**, *215*, 347 – 352.
[20] C. Ratzer, J. Küpper, D. Spangenberg, M. Schmitt, *Chem. Phys.* **2002**, *283*, 153 – 169.
[21] A. Courty, M. Mons, B. Dimicoli, F. Piuzzi, V. Brenner, P. Millié, *J. Phys. Chem. A* **1998**, *102*, 4890 – 4898.
[22] M. Schmitt, J. Küpper, D. Spangenberg, A. Westphal, *Chem. Phys.* **2000**, *254*, 349 – 361.
[23] A. Westphal, C. Jacoby, C. Ratzer, A. Reichelt, M. Schmitt, *Phys. Chem. Chem. Phys.* **2003**, *5*, 4114 – 4122.
[24] D. M. Chapman, K. Müller-Dethlefs, J. B. Peel, *J. Chem. Phys.* **1999**, *111*, 1955 – 1963.
[25] S. R. Haines, W. D. Geppert, D. M. Chapman, M. J. Watkins, C. E. H. Dessent, M. C. R. Cockett, K. Müller-Dethlefs, *J. Chem. Phys.* **1998**, *109*, 9244 – 9251.
[26] M. S. Ford, S. R. Haines, I. Pugliesi, C. E. H. Dessent, K. Müller-Dethlefs, *J. Electron Spectrosc. Relat. Phenom.* **2000**, *112*, 231 – 239.
[27] A. Fujii, M. Miyazaki, T. Ebata, N. Mikami, *J. Chem. Phys.* **1999**, *110*, 11125 – 11128.
[28] N. Solca, O. Dopfer, *Chem. Phys. Lett.* **2000**, *325*, 354 – 359.
[29] M. Schmitt, C. Ratzer, W. L. Meerts, *J. Chem. Phys.* **2004**, *120*, 2752 – 2758.
[30] J. A. Syage, J. Steadman, *J. Chem. Phys.* **1991**, *95*, 2497 – 2510.
[31] M. F. Hineman, D. F. Kelley, E. R. Bernstein, *J. Chem. Phys.* **1993**, *99*, 4533 – 4538.
[32] G. A. Pino, G. Grégoire, C. Dedonder-Lardeux, C. Jouvet, S. Martrenchard, D. Solgadi, *Phys. Chem. Chem. Phys.* **2000**, *2*, 893 – 900.
[33] G. Grégoire, C. Dedonder-Lardeux, C. Jouvet, S. Martrenchard, A. Peremans, D. Solgadi, *J. Phys. Chem. A* **2000**, *104*, 9087 – 9090.
[34] G. Grégoire, C. Dedonder-Lardeux, C. Jouvet, S. Martrenchard, D. Solgadi, *J. Phys. Chem. A* **2001**, *105*, 5971 – 5976.
[35] M. Schmitt, C. Jacoby, M. Gerhards, C. Unterberg, W. Roth, K. Kleinermanns, *J. Chem. Phys.* **2000**, *113*, 2995 – 3001.
[36] H. T. Kim, R. J. Green, J. Qian, S. L. Anderson, *J. Chem. Phys.* **2000**, *112*, 5717 – 5721.
[37] S. Ishiuchi, M. Saeki, M. Sakai, M. Fujii, *Chem. Phys. Lett.* **2000**, *322*, 27 – 32.
[38] S. Ishiuchi, K. Daigoku, M. Saeki, M. Sakai, K. Hashimoto, M. Fujii, *J. Chem. Phys.* **2002**, *117*, 7077 – 7082.
[39] S. Ishiuchi, K. Daigoku, M. Saeki, M. Sakai, K. Hashimoto, M. Fujii, *J. Chem. Phys.* **2002**, *117*, 7083 – 7093.
[40] S. R. Haines, C. E. H. Dessent, K. Müller-Dethlefs, *J. Chem. Phys.* **1999**, *111*, 1947 – 1954.
[41] K. Fuke, K. Kaya, *Chem. Phys. Lett.* **1982**, *91*, 311 – 314.
[42] K. Fuke, K. Kaya, *Chem. Phys. Lett.* **1983**, *94*, 97 – 101.
[43] O. Dopfer, G. Lembach, T. G. Wright, K. Müller-Dethlefs, *J. Chem. Phys.* **1993**, *98*, 1933 – 1943.
[44] M. Schmitt, U. Henrichs, H. Müller, K. Kleinermanns, *J. Chem. Phys.* **1995**, *103*, 9918 – 9928.
[45] K. Ohashi, Y. Inokuchi, N. Nishi, *Chem. Phys. Lett.* **1996**, *257*, 137 – 142.
[46] G. V. Hartland, B. F. Henson, V. A. Venturo, P. M. Felker, *J. Phys. Chem.* **1992**, *96*, 1164 – 1173.
[47] T. Ebata, T. Watanabe, N. Mikami, *J. Phys. Chem.* **1995**, *99*, 5761 – 5764.
[48] T. Ebata, M. Kayano, S. Sato, N. Mikami, *J. Phys. Chem. A* **2001**, *105*, 8623 – 8628.
[49] P. M. Felker, *J. Phys. Chem.* **1992**, *96*, 7844 – 7857.
[50] L. L. Connell, S. M. Ohline, P. W. Joireman, T. C. Corcoran, P. M. Felker, *J. Chem. Phys.* **1992**, *96*, 2585 – 2593.
[51] A. Weichert, C. Riehn, B. Brutschy, *J. Phys. Chem. A* **2001**, *105*, 5679 – 5691.
[52] S. Nakagawa, Y. Matsushita, T. Suzukia, T. Ichimura, *J. Mol. Struct.* **2005**, *779*, 68 – 71.
[53] T. K. Ghosh, E. Miyoshi, *Theor. Chem. Acc.* **2000**, *105*, 31 – 38.
[54] P. Hobza, C. Riehn, A. Weichert, B. Brutschy, *Chem. Phys.* **2002**, *283*, 331 – 339.
[55] W. Roth, C. Jacoby, A. Westphal, M. Schmitt, *J. Phys. Chem. A* **1998**, *102*, 3048 – 3059.
[56] O. Treutler, R. Ahlrichs, *J. Chem. Phys.* **1995**, *102*, 346 – 354.
[57] F. Weigend, M. Häser, *Theor. Chem. Acc.* **1997**, *97*, 331 – 340.
[58] F. Weigend, M. Häser, H. Patzelt, R. Ahlrichs, *Chem. Phys. Lett.* **1998**, *294*, 143.
[59] P. Deglmann, K. May, F. Furche, R. Ahlrichs, *Chem. Phys. Lett.* **2004**, *384*, 103 – 107.
[60] P. Deglmann, F. Furche, R. Ahlrichs, *Chem. Phys. Lett.* **2002**, *362*, 511 – 518.
[61] P. Deglmann, F. Furche, *J. Chem. Phys.* **2002**, *117*, 9535 – 9538.
[62] C. Huber, R. Ahlrichs, A. Schäfer, *J. Chem. Phys.* **1994**, *100*, 5829 – 5835.
[63] Gaussian 03, Revision C.02, M. J. Frisch et al., Gaussian, Inc., Wallingford, CT, **2004**.
[64] T. H. Dunning, Jr., *J. Chem. Phys.* **1989**, *90*, 1007 – 1023.
[65] R. Krishnan, J. Binkley, R. Seeger, J. Pople, *J. Chem. Phys.* **1980**, *72*, 650 – 654.
[66] O. Christiansen, H. Koch, P. Jørgensen, *Chem. Phys. Lett.* **1995**, *243*, 409 – 418.
[67] C. Hättig, F. Weigend, *J. Chem. Phys.* **2000**, *113*, 5154.
[68] C. Hättig, *J. Chem. Phys.* **2003**, *118*, 7751.
[69] A. Köhn, C. Hättig, *J. Chem. Phys.* **2003**, *119*, 5021 – 5036.
[70] S. F. Boys, F. Bernardi, *Mol. Phys.* **1970**, *19*, 553 – 566.
[71] G. Schaftenaar, J. H. Noordik, *J. Comput.-Aided Mol. Des.* **2000**, *14*, 123 – 134.
[72] MOLEKEL, S. Portmann, http://www.cscs.ch/molekel/, **2002** CSCS/UNI Geneva.
[73] http://www-public.rz.uni-duesseldorf.de/~pc1/kleinermanns/publikationen2007.html.

Received: February 20, 2007
Published online on May 18, 2007

